A topological study of chemical bonds under pressure: solid hydrogen as a model case

Vanessa Riffet, Vanessa Labet, Julia Contreras-García

▶ **To cite this version:**

Vanessa Riffet, Vanessa Labet, Julia Contreras-García. A topological study of chemical bonds under pressure: solid hydrogen as a model case. Physical Chemistry Chemical Physics, 2017, 19 (38), pp.26381 - 26395. 10.1039/C7CP04349J . hal-01613197

HAL Id: hal-01613197

https://hal.sorbonne-universite.fr/hal-01613197

Submitted on 9 Oct 2017

HAL is a multi-disciplinary open access archive for the deposit and dissemination of scientific research documents, whether they are published or not. The documents may come from teaching and research institutions in France or abroad, or from public or private research centers.

L'archive ouverte pluridisciplinaire **HAL**, est destinée au dépôt et à la diffusion de documents scientifiques de niveau recherche, publiés ou non, émanant des établissements d'enseignement et de recherche français ou étrangers, des laboratoires publics ou privés.

Topological study of chemical bonds under pressure: solid hydrogen as a model case

Vanessa Riffet [a]†*, Vanessa Labet [b*], Julia Contreras-García [a]

[a] *Sorbonne Universités, UPMC Univ Paris 06, CNRS, Laboratoire de Chimie Théorique (LCT), 4 place Jussieu F-75005 Paris, France*

[b] *Sorbonne Universités, UPMC Univ Paris 06, CNRS, Laboratoire de la Molécule aux Nano-objets : Réactivité, Interactions et Spectroscopies (MONARIS), 4 place Jussieu F-75005 Paris, France*

Corresponding author:

vanessa.riffet@laposte.net **; vanessa.labet@upmc.fr**

Abstract.

It is now well recognized that a fundamental understanding of the rules that govern chemistry under pressure is still lacking. Hydrogen being the "simplest" element as well as a central core to high pressure physics, we undertake a general study of the changes in the chemical bonding under pressure. We start from a simple trimer unit that has been found in high pressure phases, whose behavior has been found to reveal the basics of hydrogen polymerization under pressure. Making use of bond analysis tools, mainly the NCI (noncovalent interactions) index, we show that polymerization takes place in three steps: dipolar attraction, repulsion and bond formation. The use of a 1D Wigner Seitz radius allowed us to extend the conclusions to 3D networks and to analyze their degree of polymerization. On the one hand, this approach provides new insight into the polymerization of hydrogen. On the other hand, it shows that complicated molecular solids can be understood from cluster models, where correlated methods can be applied, main differences in solid state arising at the transition points, where breaking/forming of bonds happens at once instead of continuously

like in the cluster model.

1. Introduction

Under pressure, properties of a material can get radically different from what they are at ambient pressure.[1] For example, any material insulating at P = 1 atm is expected to turn metallic if submitted to a high enough pressure.[2] Maybe more appealing, unusual states of matter, such as superconductivity, can become quite common.[3] Concomitantly, the network of chemical bonds ensuring the cohesion of matter can get quite transformed as well as their very nature can change radically. As an example, weak intermolecular bonds that maintain together the molecules of a molecular solid can transform into strong "intramolecular" bonds under pressure, as the monomeric molecules that constitute the solid at low pressure polymerize into a 3D extended network of covalent bonds upon compression.[4] Typical examples are N_2 [5] and CO_2 [6] which are well known to form molecular solids at ambient pressure and transform into polymeric structures where N and C atoms are 3- and 4-coordinated at high pressure, respectively. These new coordinations correspond to those of P and Si in solid P and solid SiO_2 at atmospheric pressure. This is an illustration of the 9th Prewitt and Downs' rule of thumb which stipulates that *elements behave at high pressures like the elements below them in the periodic table at lower pressures*.[7] Despite the establishment of many such rules, Hemley pointed out that '*a fundamental yet empirically useful understanding of how pressure alters the chemistry of the elements is lacking*'.[8] Therefore, pursuing the effort to build solid foundations for our chemical intuition under pressure is essential. In this perspective, understanding the behavior of hydrogen, the 'simplest' of the elements, under pressure appears as one of the most logical thing to do. Furthermore, hydrogen could have been very recently metallized,[9] though this result is still controversial.[10]

Following the argument mentioned above, hydrogen which forms a molecular solid at ambient pressure has long been expected to transform under pressure into a body-centered cubic (bcc) lattice of hydrogen atoms (analogue to those of other alkali metals) which would

exhibit metallic properties.[2] This marked the starting point for the long quest for metallic hydrogen,[11] which was predicted to be a high-temperature superconductor[12-14] and a metallic superfluid.[15,16] Since then, some recent studies suggest a coordination number of 3 or 4 rather than 8 for the atomic phase of hydrogen.[17-20] And the Wigner-Huntington transition could have been finally found in diamond anvil cells experiments though it remains to be confirmed.[9,10] The main goal of the work presented here is to set the bases for a quantitative chemical characterization of the bonding network transformation upon polymerization, as cohesion in the solid changes from purely long-range electrostatic and van der Waals interactions between fragments (molecular phases) to covalency.

Experimentally, useful information about the response of H-H intramolecular bonds and H_2---H_2 intermolecular interactions upon static compression in diamond anvil cells have been brought by vibrational spectroscopies, both infrared and Raman.[21,22] These techniques allowed identifying at least three phases for hydrogen at low temperatures, the so-called phases I, II and III, all of them molecular. At higher temperature, another molecular phase has been observed, known as phase IV. At low temperatures H_2 molecular entities persist well above P = 300 GPa.[23] The Raman vibron frequency characteristic of the H_2 molecular entity first increases from 1 atm to around 50 GPa and then decreases up to 320 GPa (with a discontinuity at the phase II → III transition). It indicates that the H-H intramolecular bond is first strengthened and then softened as intermolecular interactions increase.[24]

Computationally, the study of the evolution of the H-H interatomic distances -- both intramolecular and intermolecular -- in periodic or not structural models proposed for dense hydrogen under pressure showed that the intramolecular H-H bond length under pressure goes through 3 successive regimes. First, the H_2 bond length is shortened as the pressure increases. Then it elongates and finally shortens again (see [25] for further details on bond length values). This has been attributed to the concomitance of two phenomena having opposite

effects: (*i*) one more physical is associated to a confinement effect due to neighboring H_2 molecules coming closer and closer as the pressure increases and which tends to shorten the H-H intramolecular distance ; and (*ii*) the other one more chemical corresponds to some charge transfer from the filled molecular orbitals (MO) of one H_2 molecule to empty MO of neighboring H_2 molecules (and *vice versa*), and which tends to weaken and elongate the H-H intramolecular bonds while H_2-H_2 intermolecular bonds are strengthened and shortened.[26,27]

Here we propose to pursue the analysis of the response of chemical interactions in these structural models for dense hydrogen (see section 2) as the pressure increases making use of tools particularly suitable to characterize chemical bonds (see section 3). All results will be summarized at the end of the paper (see section 4).

2. Structural models for dense hydrogen under pressure

a) Periodic models

During the last decade, several studies have been dedicated to the search of good candidate structures for the experimentally observed phases of dense hydrogen, mainly based on DFT computations.[18-20,28-30] We can cite in particular the pioneering work performed by C. J. Pickard and R. J. Needs using Ab Initio Random Structure Searching (AIRSS).[31] In their study, they proposed several candidates for the structure of dense hydrogen under pressure from 1 atm to P = 500 GPa, with focus on the pressure regime of phase III (from P = 150 GPa to at least P = 320 GPa). In particular, five structures are successively proposed to be that of lowest enthalpy at T = 0 K as the pressure increases (see Table 1). The *$P6_3/m$*, *C2/c*, *Cmca-12* and *Cmca* phases are all molecular and can be described as layered, a layer of each being shown in Table 1. The 5th one, of *$I4_1/amd$* symmetry, can be described as monoatomic and

involves 4-fold coordinated hydrogens (see Table 1). These are the structures for which we followed the evolution of the shortest (intramolecular) and second shortest (intermolecular) H-H distances under pressure in a previous study.[25] Since then, better candidates than *P6$_3$/m*, *Cmca-12* and *Cmca* have been proposed in their respective range of stability.[30] Nonetheless, it has to be emphasized that all these molecular structures are quasi-energetic; they only differ by a few tens of meV per proton. This small difference is due to the fact that the interactions ensuring their respective cohesions are basically the same. And in this work, we will show that the response of chemical bonds to an increase of pressure is qualitatively the same for each of these molecular structures.

Table 1. Most stable **structures** extracted from [19] for solid hydrogen under at each pressure range **P** up to P = 500 GPa, within the static lattice approximation. **Symmetry** collects the symmetry of each of the structures, H coordination number being noted **n**. In the *P*6$_3$/*m*, *Cmca*-12 and *Cmca* structures the layers are arranged in an ABA fashion; in the *C*2/*c* structure they are arranged in an ABCDA fashion. Crystal structures have been plotted by using the Visualization for Electronic and Structural Analysis (VESTA) software package.[32]

P	Symmetry	n	Structure
< 105 GPa	*P6$_3$/m*	1 (molecular)	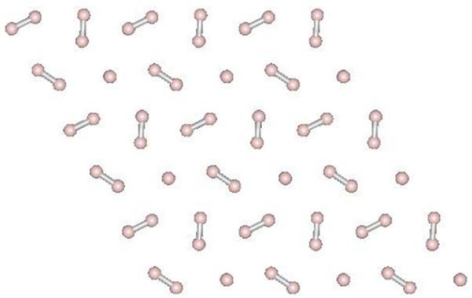

105 - 270 GPa	*C2/c*	1 (molecular)	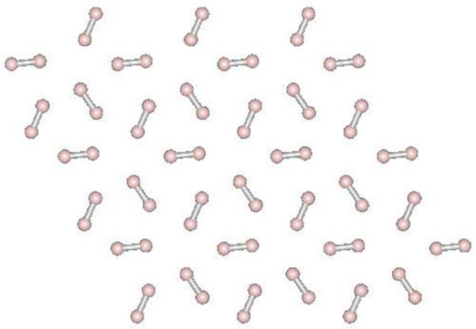
270 - 385 GPa	*Cmca-12*	1 (molecular)	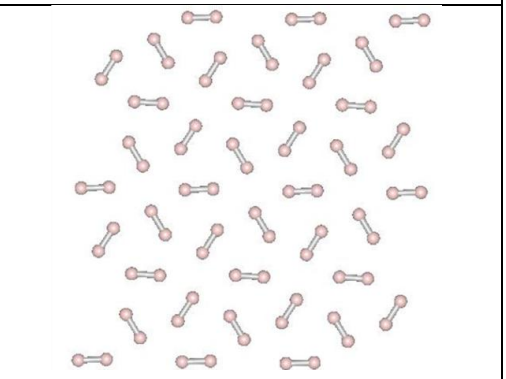
385 - 490 GPa	*Cmca*	1 (molecular)	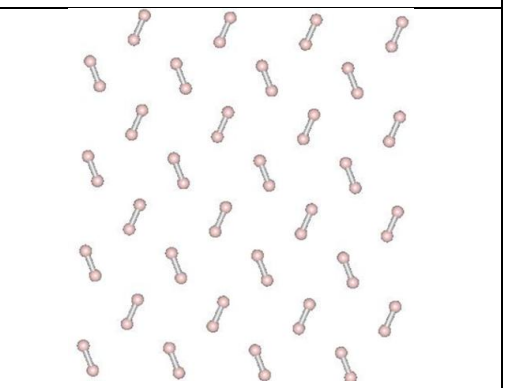
> 490 GPa	*I4$_1$/amd*	4 (monoatomic)	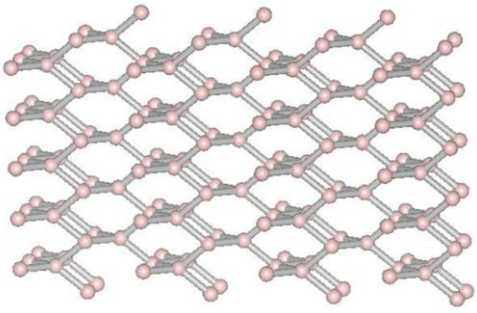

b) Molecular model $3H_2$

Interestingly, a more or less symmetric ring of 3 H_2 molecules can be found in the *P6$_3$/m*, *C2/c* and *Cmca-12* phases (see Table 1). It is also present in the *Pc-48* structure which has

been proposed by Drummond *et al.* to be a good model for phase IV (see [30] for details on the structure).

This non-periodic system has been studied by itself in our recent study where a neutral assembly of 6 protons and 6 electrons was confined in the perimeter of a ring.[26] Overall this system was fixed to a D_{3h} point-group symmetry, and the pressure exerted on it was simulated by decreasing the value of the ring radius d (see Figure 1).[33] Constrained to keep this D_{3h} symmetry, the intramolecular $r_{H\text{-}H}$ and intermolecular $R_{H2\text{-}H2}$ distances were optimized for each imposed value of the d parameter. Very interestingly, this simple model contained the physics of the solid system. The intramolecular $r_{H\text{-}H}$ distances first decreased, then increased, and then decreased again as d was decreased in the calculation. Just alike the intramolecular H-H distances in 3D periodic models for dense hydrogen under pressure.[25] Therefore, this very simple model contains all the ingredients to study the polymerization process for dense hydrogen under pressure.

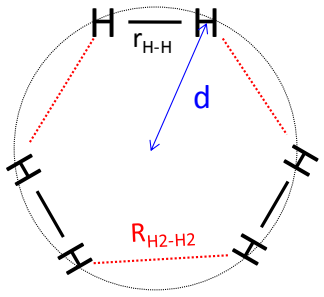

Figure 1. "3 H_2" molecules confined in a ring and constrained to D_{3h} symmetry, the distance d being adjusted to model the effect of pressure.

Thus, we first decided to pursue the analysis of the chemical bond networks under pressure in this simple non-periodic model, using tools specifically designed for the study of chemical bonds (see section 3). To present our results, we will introduce an analogue of a quantity very

commonly used within high pressure, the dimensionless Wigner-Seitz radius, that we will note $r_{s,1D}$ (r_s for brevity) and which we define as follows:

$$2\pi d = 6(2r_{s,1D}a_0) \quad (1)$$

where a_0 is the Bohr radius.

The non-periodic results obtained, constituting the core of our study, are presented in section 5.a. Then, in order to check their general character, using the same analysis tools, we will look at periodic models for dense hydrogen under pressure, i.e. the *P6₃/m*, *C2/c*, *Cmca-12*, *Cmca* and *I4₁/amd* structures mentioned above, in the pressure range for which they have been proposed to be the best ones in the original paper of Pickard and Needs.[19] The periodic results are presented in section 5.b.

3. Theoretical background: Bond analysis

Over the years, different approaches have been developed to characterize the chemical bond and its changes. One of the first indices used in this respect was the bond order, which enabled to recover a very established criterion in classical chemistry from quantum mechanical grounds. Developed to quantify the process of bond formation, the bond order recovered the concept of bond multiplicity. Its variation along a reaction enables to visualize the electronic reorganization in terms which are very close to chemical intuition.

At the Hartree-Fock level, the Wiberg bond index,[34] WBI_{AB}, probably constitutes the most well-known bond order index:

$$WBI_{AB} = \sum_{\mu \epsilon A} \sum_{\nu \epsilon B} |P_{\mu\nu}|^2 \quad (2),$$

where $P_{\mu\nu}$ is the matrix for Atomic Orbitals μ and ν, running over the atomic centers A and B.

Although these indices have known a good deal of acceptance, there is not a unique definition for correlated cases. Moreover, they can sometimes lead to confusing or misleading situations, especially if diffuse orbitals are used.

However, the MO dimensions (Hilbert space) need clearly to be reduced to retrieve a clear picture of the bond formation. One of the techniques that have been introduced in the last decades to reduce the dimensionality of the problem is the topological approach. 3D space is divided into mutually disjoint regions following the gradient of a scalar function. Depending on the function, different partitions arise. We will be resorting to three different functions: ELF, NCI and the electron density itself.

Quantum Theory of Atoms In Molecules (QTAIM)

The analysis of the topology of the electron density can provide a wealth of information on the evolution of bonds.[35] Most typically, the first order saddle points of the electron density are associated with the existence of a bond/interaction between the atoms it joins together (this is the reason why they are also known as bond critical points). The changes in the value of the electron density at these points can be used to understand density accumulation or depletion under pressure.

QTAIM can be further used to decompose the total energy of a many-electron system into intra- and interatomic terms, in what is known as the Interacting Quantum Atoms scheme (IQA). It provides energetic terms associated with the AIM basins, which can be divided in self (one-basin) terms or interaction in between several basins. Many qualitative ideas about

the Pauli principle and repulsion can be quantified using this scheme from the deformation of the atoms within the multiatomic system as compared to the free atoms.

Electron Localization Function (ELF)

ELF topological analysis divides the space into chemically intuitive regions associated with electron pairs so that electron shells, bonds and lone pairs are revealed.[36,37]

ELF may be understood in terms of the excess of local kinetic energy density due to Pauli repulsion:

$$ELF = \frac{1}{1+\chi^2} \quad (3)$$

$$\chi = \frac{t_P(\vec{r})}{t_{HEG}(\vec{r})} \quad (4),$$

where $t_P(\vec{r}) = t(\vec{r}) - \frac{1}{8}\frac{|\nabla^2\rho|}{\rho}$ (5) is the excess of local kinetic energy density due to the Pauli principle and $t_{HEG}(\vec{r}) = c_F\rho^{5/3}$ (6) is the kinetic energy density associated with a homogeneous electron gas (HEG) of electron density ρ with c_F the Fermi constant. For our case, it should be noted that since there are no same spin electrons in the hydrogen molecule, ELF is not very informative on the H_2 covalent bond itself, however*, its shape can still provide information on the polarization of the molecules*. If the ELF shape deforms towards a neighboring molecule, a stabilizing polarization is being revealed. If instead a retreat is found, it can be understood as the presence of repulsion between neighbors.

Non-Covalent interactions Index (NCI)

Since ELF is not enough to analyze the H_2 molecule we will also resort to the NCI index revealing the formation of bonds, from weak to covalent interactions.[38] NCI provides a rich

representation of attractive interactions, such as van der Waals interactions or hydrogen bonds, and steric repulsions.

NCI maps non-covalent interactions using a reduced gradient (s(ρ)) based on the electron density and its derivatives:[39]

$$s(\rho) = \frac{|\nabla\rho|}{c_F\rho^{4/3}} \quad (7)$$

It is a dimensionless quantity used in DFT to describe the deviation due to interactions. In density tails (i.e. regions far from the molecule, in which the density is decaying to zero exponentially), s(ρ) achieves very large positive values. On the contrary, s(ρ) assumes very small values, approaching zero, for regions of both covalent bonding and non-covalent interactions.

These low s(ρ) areas are traced back to molecular space giving rise to isosurfaces that enable to visualize the interactions in the system. It is possible to separate the attractive and repulsive contributions depending on the sign of the second eigenvalue (λ_2) of the electron-density Hessian matrix at each point: Hydrogen bonds appear at negative values of λ_2, while repulsion appears at positive values and dispersion at values close to zero. Using this information (sign(λ_2)ρ) to color the isosurfaces, we can differentiate all the interactions. We will use the following color code: the covalent bonds and highly attractive weak interactions (e.g. hydrogen bonds) are in blue, extremely weak interactions (such as very weak H-H interactions or dispersive-like van der Waals) are in green and repulsive interactions (such as steric clashes) are in red.

A new version of the NCIPLOT program has been used to integrate density properties within the NCI region to obtain the volume (V_{NCI}) enclosed within the NCI volume.[40,41]

$$V_{\mathrm{NCI}} = \int_{\Omega_{\mathrm{NCI}}} \mathrm{d}\,\vec{r} \quad (8)$$

To perform such integrations, it is necessary to establish a unique definition of the NCI volume. Because the difference between the interacting and non-interacting monomers is directly reflected in the $s(\rho)$ diagram, it is possible to define the NCI region as the points in 3D space with (ρ, s) values lying in the $s(\rho)$ peak. To identify this region, the isolated monomer (ρ, s) values are approximated from the total wavefunction and the lower edge of the pseudo-monomer *s(ρ)* curve is splined. All the points of the interacting monomers *s(ρ)* plot lying below the splined curve are localized in real space. In our case, we have used the H_2 molecules at each r_s as reference.

In the next sections we used a wealth of bond analyses, in Hilbert and real space, to reveal the extent of the polymerization, *i.e.* the discrimination between molecular and non-molecular phases.

4. Computational details

a) Molecular model $3H_2$.

The obtained geometries were optimized with the Gaussian09, Revision D.01 program package using the PBEPBE functional along with the 6-311++G(d,p) basis set under geometrical constraints, i.e. by freezing *d* and letting the rest of the parameters (among which $R_{H2\text{-}H2}$ and $r_{H\text{-}H}$) optimize under the symmetry group.[42] *d* took values ranging from 2.2 Å to 0.75 Å. A ring radius of *d* = 2.2 Å led to intermolecular $R_{H2\text{-}H2}$ distances longer than those found in solid hydrogen at low temperature and P = 1atm. On the contrary, a ring radius of *d* = 0.75 led to intermolecular $R_{H2\text{-}H2}$ distances exactly equal to intramolecular $r_{H\text{-}H}$ ones. Thus,

the chosen range of *d* values completely covers the hydrogen polymerization process we aim to study.

The dispersion energy is well-known to be not directly included in standard DFT which therefore fails in recovering correct intermolecular distances for van der Waals complexes / solids in unconstrained optimization procedures. However, for a given geometry, DFT will essentially give the correct corresponding electron density, the physical quantity which is of particular interest here. Note that there exist many dispersion corrections which can be included a posteriori, on-top of densities obtained from local exchange-correlation functionals.[43,44] One may argue that the resulting configurations may not be those of lowest energies. Nonetheless, the fact that this very simple structural model studied by DFT was able to reproduce the non-monotonous behaviour of intramolecular H-H distances under pressure reinforces us in the idea that our methodology contains all the requisite ingredients to gain qualitative insight on the response of chemical bonds / interactions to an increase of pressure.[26]

It should be noted that densities show very little dependency on the method of calculation. Moreover, some of the indexes used (ELF) are not uniquely defined for post-HF methods. Hence, DFT densities are a good compromise of correlated monodeterminental densities leading to virtually no topological differences with respect to post-HF densities. Instead, for the quantification of charge transfer from bonding to antibonding MOs as the *d* parameter decreases, multiconfiguration *ab initio* calculations were performed thanks to the MOLPRO program package with the cc-pVQZ basis set.[45,46] CASSCF geometries were fixed to the PBEPBE results for a coherent description of the system and the subgroup fixed to C_{2v} since only Abelian point group symmetries are available in MOLPRO.

The Wiberg bond indices (WBI) have been calculated using PBEPBE/6-311++G(d,p) and the natural population analysis method implemented in the Gaussian09, Revision D.01 program package.[34,42]

The ELF and QTAIM interpretative analyses were performed using the TopMod software.[47]

For the NCI analyses, SCF densities were considered and the NCIPLOT software version 1.0 was used.[38,40] The increments along the x, y and z directions of the cube were set to 0.05, 0.05 and 0.05 a.u., respectively. Integrations of density properties within the NCI regions were performed numerically, by summation over a cubic grid with 0.1 a.u. increments, with the H_2 molecules in the trimer geometry as reference.

b) Periodic models.

Geometries

In the present study, the projector augmented plane-wave (PAW) method was used as implemented in the Vienna ab initio Simulation Package (VASP) code.[48-52] We optimized the ground state static structures starting from the structures obtained by Pickard and Needs for pressures ranging from 0 to 2000 GPa using the Perdew-Burke-Ernzerhof (PBE) generalized gradient approximation density functional with a pseudopotential cutoff radius of $0.8a_0$ and a cutoff of 2000 eV for the kinetic energy.[53] K-points were sampled using the Monkhorst-Pack scheme with a grid of spacing of $2\pi\times0.02$ Å^{-1}.

Topological post-analysis

For all phases, the periodic solid-state electron densities were considered and used for the NCI analysis as implemented in the CRITIC2 Version 1.0 program.[54] The cubic grid was set to 0.001, 0.001 and 0.001 a.u. along each axis.

5. Results and discussion

1. Ring of 3 H_2 molecules.

a. A quick reminder of what we already know

As we mentioned above, we essentially chose to study the non-periodic "$3H_2$" system as it can be considered the simplest model for dense hydrogen that contains all the ingredients to study the pressure induced polymerization process. This assertion arises from the analysis of the evolution of H-H distances as the r_s parameter decreases. Figures 2.a and 2.b show the evolution of $r_{H\text{-}H}$ and $R_{H2\text{-}H2}$ as r_s decreases. Intermolecular distances, $R_{H2\text{-}H2}$, decrease as the pressure increases (modelled by a decrease of r_s). $R_{H2\text{-}H2}$ evolves almost linearly with r_s. It decreases from 3.90 Å to 0.75 Å as r_s decreases from 2.50 to 0.75.

As mentioned above, the evolution of $r_{H\text{-}H}$ is more complex. It first decreases slightly (from 0.752 Å to 0.747 Å) as r_s decreases from 2.50 to 1.25. Then it increases from 0.747 Å to 0.89 Å when r_s decreases from 1.25 to 0.90. Finally, it decreases again from 0.89 Å to 0.75 Å upon a decrease in r_s from 0.90 to 0.75. Globally, on the first two regimes, i.e $0.90 < r_s < 2.50$, $r_{H\text{-}H}$ is essentially constant and identical to the H-H bond length of an isolated H_2 molecule for r_s from 2.50 to 2.00. Then $r_{H\text{-}H}$ of the H_2 entities of the "3 H_2" system are shorter than that of an isolated molecule (r_s from 2.0 to 1.1) and finally they become longer (r_s from 1.1 to 0.90).

To measure the degree of equalization of intra- and inter-molecular H-H separations, we introduced in a previous study,[25] an equalization index noted ξ_{3H2} (r_s), or ξ for brevity:

$$\xi = 1 - \frac{R_{H2-H2}(r_s) - r_{H-H}(r_s)}{R_{H2-H2}(P_{1atm}) - r_{H-H}(P_{1atm})} \quad (9)$$

where $R_{H2\text{-}H2}(P_{1atm})$ and $r_{H\text{-}H}(P_{1atm})$ are the shortest and second shortest H-H separations at P = 1 atm (0.751 and 3.105 Å, respectively) extracted from [25].

Its evolution for the $3H_2$ system is shown in Figure 3. For $r_s > 1.1$, it evolves almost linearly with r_s. For $r_s > 2.0$ it is negative, which indicates that for those values of r_s, the intermolecular distances are longer than in solid hydrogen at P = 1atm. In other words, these r_s values model a pressure smaller than P = 1atm, and are of little interest for us. For $r_s < 0.9$, ξ=1 which indicates that intramolecular $r_{H\text{-}H}$ and intermolecular $R_{H2\text{-}H2}$ distances have become equal. The system is polymerized.

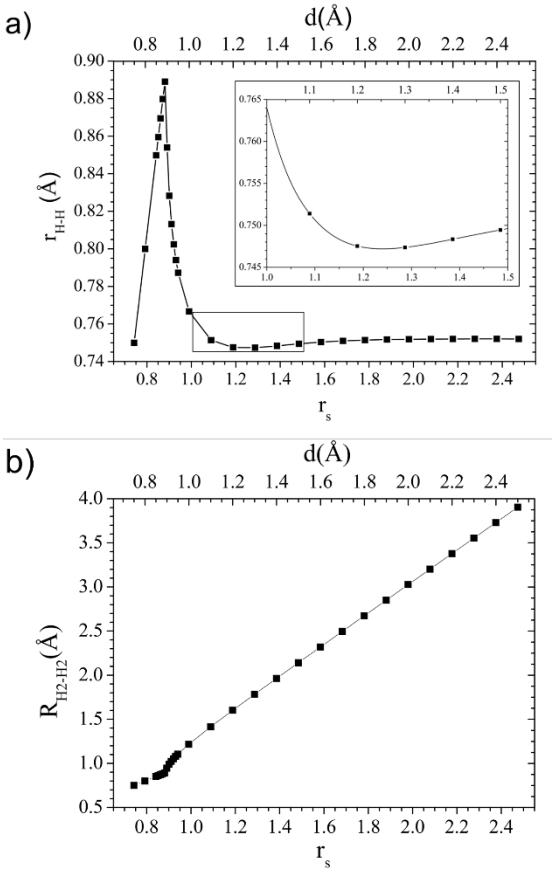

Figure 2. Evolution of the a) r_{H-H} and b) R_{H2-H2} as a function of dimensionless Wigner-Seitz radius (r_s).

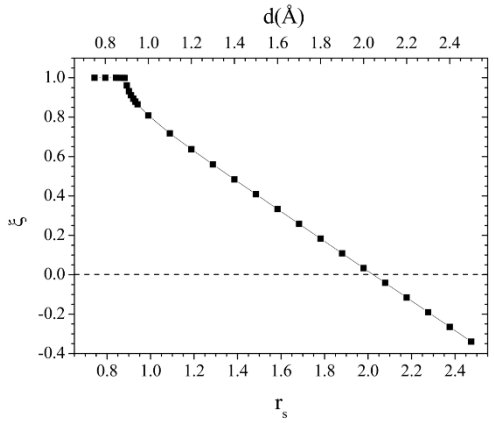

Figure 3. Evolution of the equalization index (ξ) with the dimensionless Wigner-Seitz radius (r_s).

The elongation of the intramolecular H_2 bond length, for $0.90 < r_s < 1.25$, has been attributed to charge transfer from bonding MOs on one H_2 molecular entity to antibonding MOs as neighboring H_2 molecules are coming closer and closer. Indeed, Figure 4 shows the evolution of the electronic population of the bonding and antibonding MOs of the H_2 molecular entities in CASSCF calculations. As r_s decreases, bonding H_2 MOs are depleted in favour of antibonding H_2 MOs. The same idea is conveyed by the evolution with r_s of the Wiberg bond index between H-H pairs separated by a r_{H-H} distance and between H-H pairs separated by a R_{H2-H2} distance (see Figure 5). Indeed, the Wiberg bond index of H-H pairs at r_{H-H} decreases from 1.00 to 0.44 as r_s decreases while that of H-H pairs at R_{H2-H2} increases from 0 to 0.44. Note that for $r_s < 0.90$, i.e the r_s regime for which r_{H-H} and R_{H2-H2} are equal, Wiberg bond indices of both kinds of H-H pairs are obviously equal too.

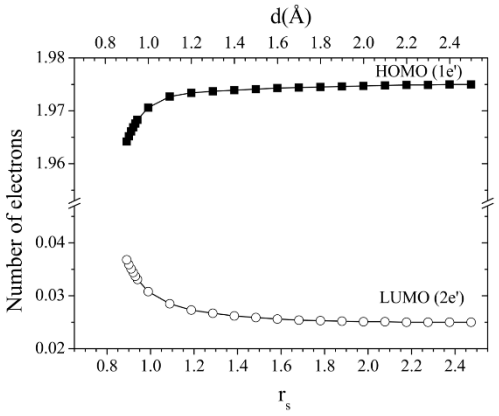

Figure 4. Evolution of the electron population of the bonding and antibonding MOs of the H-H pairs separated by r_{H-H} as a function of r_s. Data were calculated using the CASSCF/cc-pVQZ level.

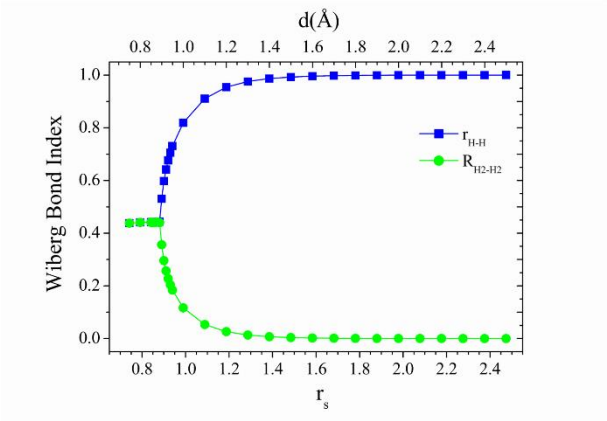

Figure 5. Natural Atomic Orbitals Wiberg bond index associated with the "3 H_2" system.

To sum up, both the equalization index (Figure 3) and the Wiberg bond indices (Figure 5) allow an easy identification of the moment where complete polymerization is reached. In the current study, we propose to go one step further and analyze this process. We want to focus on the polymerization itself and characterize the steps leading to it. We are particularly interested in the transition from a system where we can speak of H_2 molecules interacting while preserving their integrity to a system where we cannot speak of H_2 molecules any longer. We will see that it occurs way before complete equalization of r_{H-H} and R_{H2-H2}.

b. Identification of the interactions present in the system.

Besides geometrical criteria, NCI analysis provides us with information on the nature of the interactions ensuring the cohesion of the system we are interested in. Figure 6 shows the NCI results for our "3 H_2" molecular model at $r_s = 2.5$, i.e. for an r_s value which can be associated with a very low pressure, lower than 1 atm, as indicated by $\xi(r_s = 1.5) < 0$. Three different regions are observed, numbered 1 to 3 on Figure 6. Region #1 has a strong attractive character (strong density and negative λ_2, $\text{sign}(\lambda_2)\rho$ = -2.56 a.u.). In the 3D picture, this is depicted as a blue isosurface. It corresponds to the intramolecular H-H covalent bonds. Two other regions, #2 and #3, appear close to each other at a very low electron density and thus are

associated with van der Waals interactions. One is attractive ($\lambda_2 < 0$ for BCP #2); it is located at the intermolecular regions between two H_2 molecules (isosurfaces in green). The other one is repulsive ($\lambda_2 > 0$ for BCP #3), located at the center of the ring (isosurfaces in green).

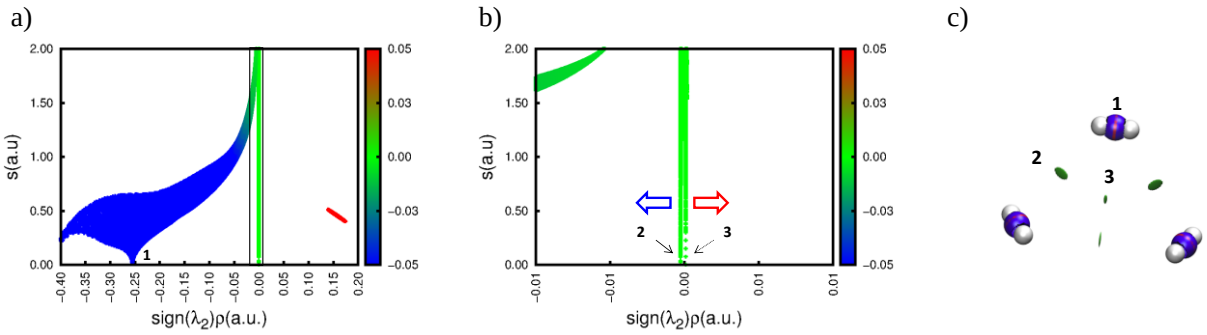

Figure 6. NCI results for our molecular model at $r_s = 2.5$. a-b) Plot of $s(\text{sign}(\lambda_2)\rho)$. b) is a zoom of a) around $\text{sign}(\lambda_2)\rho = 0$ a.u. c) NCI isosurfaces for s=0.5. The meaning of the surfaces is described in the text.

c. Global Evolution of the interactions with pressure - The NCI and ELF pictures

As mentioned previously, the "pressure" imposed to the "3 H_2" molecular model is simulated by decreasing the r_s parameter value. Figure 7 shows the evolution with r_s of the $\text{sign}(\lambda_2)\rho$ value characteristic of each of the three interactions identified previously (Figure 6), the absolute value of which informs on the strength of the interaction.

As r_s decreases, from 2.5 to 0.75, the absolute value of $\text{sign}(\lambda_2)\rho$ increases at the bond critical point characteristic of interaction #2 and at that characteristic of interaction #3, both identified as van der Waals interactions at high r_s value. The evolution is slow for $1.2 < r_s < 2.5$ and then more abrupt. This is in agreement with the idea that as r_s decreases, intermolecular interactions strengthen. Thus, the attractive interaction between H_2 entities becomes more and more attractive while the repulsive interaction associated with the ring bond critical point (the center of the ring) becomes more and more repulsive. We can note that

if the evolution of sign(λ_2)ρ is smooth for interaction #3 (repulsive), it is not the case for interaction #2 (attractive). Indeed there is a cusp at r_s = 0.90, the r_s value at which r_{H-H} and R_{H2-H2} become equal. Interestingly, the electron density at the bond critical point characteristic of interaction #3 (repulsive) is always lower than that associated to stabilizing interactions, which can be taken as a sign of the favorable nature of the polymerization process.

Concomitantly, the value of ρ at the covalent bond critical point first increases very slightly (from 0.255 to 0.259 a.u.) as r_s decreases from 2.5 to 1.2. Then it decreases (from 0.256 to 0.173 a.u.) when r_s decreases from 1.2 to 0.90. So, from r_s = 2.50 to r_s = 2.00, the electron density at the BCP of intramolecular bonds is almost constant and identical to the characteristic value of an isolated H_2 molecule. From r_s = 2.0 to r_s = 1.1, it is higher than in reference normal isolated H_2 molecule and then from r_s = 1.1 to r_s = 0.90 it is lower. Finally ρ at the bond critical point of covalent bonds increases again (from 0.177 to 0.249 a.u.) as r_s decreases from 0.90 to 0.75 (see Table S1 in S.I). This is in agreement with H-H intramolecular bonds being strengthened then softened and then strengthened again as H_2 molecular entities are coming closer together (section 5.1.a).

Note that below r_s = 0.90, sign(λ_2)ρ takes the same value at the bond critical point of interactions #1 and #2, which is consistent with the fact that on this r_s domain, “intramolecular” and “intermolecular” bonds are no longer distinguishable, the system being completely polymerized. So for r_s < 0.90, the system should be considered as an H_6 molecular entity made of 6 covalent bonds rather than as a complex made of 3 H_2 molecules.

For illustrative purposes, Figure 8 shows NCI and ELF isosurfaces for representative r_s values. The strengthening of intermolecular interactions as r_s decreases translates into bigger and bigger NCI isosurfaces. In the “intermolecular” region the color progressively changes from green to blue and red meaning that intermolecular interactions, identified as van der

Waals interactions at "high" r_s values, are becoming covalent bonds. For $r_s < 0.90$, the form of the NCI isosurfaces clearly indicates that the six H---H interactions are similar and that the system is polymerized. The shape of ELF isosurfaces is particularly informative. As r_s decreases from 2.5 to 1.2, the quasi-prolate shape of the surfaces around the three H_2 molecular entities is deforming towards the center of the ring. It indicates that H_2 entities are polarizing to "avoid" neighboring H_2 molecules. The inverse deformation is then observed from $r_s = 1.1$ to $r_s = 0.90$ with a retreat in the zone between the two H of H_2 entities which indicates that H_2 entities are feeling repulsion from their neighbors. For $r_s < 0.90$, there is no longer any difference from the ELF point of view between H-H pairs distant of r_{H-H} and H-H pairs distant of R_{H2-H2}.

We can be more precise about the moment when H_2 molecular entities are losing their integrity. In the coming section we concentrate on the r_s regime preceding complete polymerization ($r_s > 0.90$). We will show that it is possible to differentiate 3 successive regimes that we will call dipolar attraction, repulsion and bond formation.

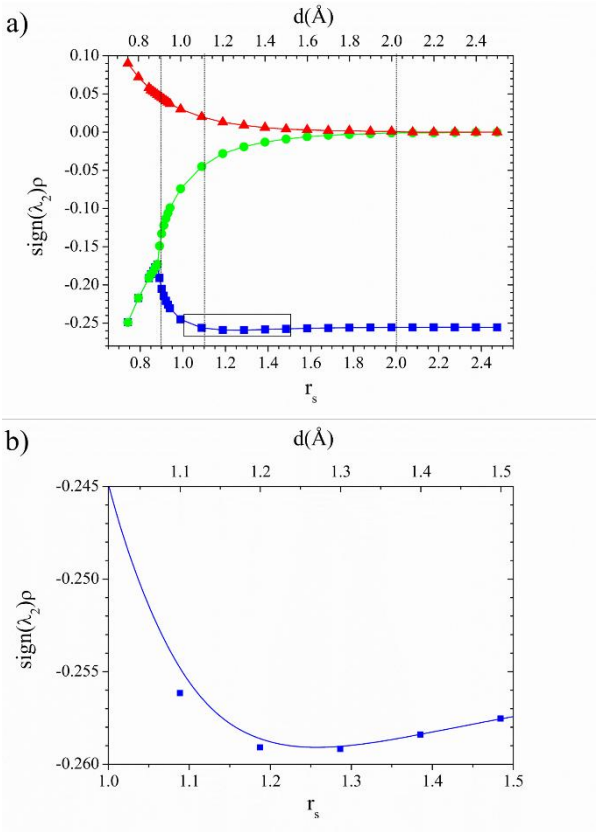

Figure 7. (a) Evolution of interactions 1 (blue), 2 (green) and 3 (red) with r_s. Vertical lines are included as guide for the eyes to highlight bonding phases. (b) zoom of (a) for r_s in the range [1.00-1.50].

r_s	**0.75**	**0.90**	**0.95**	**1.10**	**1.30**	**1.50**	**2.50**
NCI	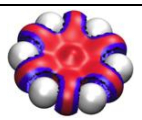	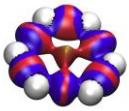	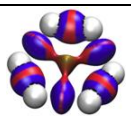	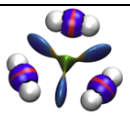	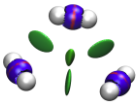	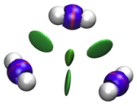	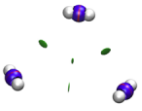
ELF	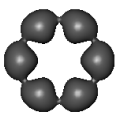		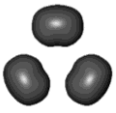	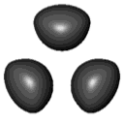	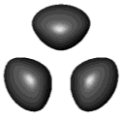	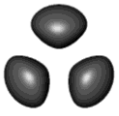	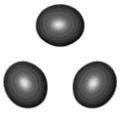

Figure 8. NCI and ELF isosurfaces for representative r_s values. NCI isosurfaces were generated for s = 0.5 a.u. and colored over the range $-0.05 < \text{sign}(\lambda_2)\rho < 0.05$. ELF isosurfaces were generated for ELF = 0.95.

d. Going in deeper details - The interaction region

As mentioned in section 3, one of the strengths of NCI is that it allows a unique definition of the NCI region in a system consisting of several monomers in interaction. This region is defined by comparing the s(ρ) diagram of the interacting system and the s(ρ) diagram of an isolated monomer. In our case, the isolated monomer will be an isolated H_2 molecule whose bond length is adapted to correspond to the $r_{H\text{-}H}$ distance characteristic of each r_s value.

The first interesting thing to do is to compare the strength of the H-H intramolecular bond in the interacting system and in the adapted isolated H_2 molecule. Figure 9 shows the difference between $\text{sign}(\lambda_2)\rho$ at the bond critical point of H-H "intramolecular" bonds in the "3 H_2" system and $\text{sign}(\lambda_2)\rho$ at the bond critical point of H-H "intramolecular" bonds in the isolated adapted H_2 molecule. This comparison enables to consider the effect of the neighboring molecules without the internal reorganization introduced by the change in covalent bond length.

From $r_s = 2.5$ to $r_s \sim 1.6$, the difference is almost zero, indicating that the H-H intramolecular bonds in the "3 H_2" system are the same as in the adapted isolated molecule. In other words, in this r_s regime, we can speak of true H_2 molecules. Nonetheless, it is interesting to note that from $r_s = 2.5$ to $r_s = 2.0$ they are identical to unperturbed H_2 molecules while from $r_s = 2.0$ to $r_s = 1.6$ they are identical to "shortened" H_2 molecules. So, from $r_s = 2.5$ to $r_s = 2.0$, the H_2 molecules of the "3 H_2" system don't see each other, in agreement with the fact that we already noticed that these r_s values could be associated with pressures lower than 1 atm. Besides, from $r_s = 2.0$ to $r_s = 1.6$, the H_2 molecules now see each other and as a consequence contract. Nevertheless, their electronic distribution appears similar to that of an isolated contracted H_2 molecule. We can thus speak of *perturbed true H_2 molecules*.

Then, from $r_s = 1.6$ to $r_s = 1.1$, the difference is low but negative. While having the same bond length, the density at the intramolecular bond critical point is therefore higher in the

interacting system than in the isolated molecule. It demonstrates an electronic distribution different from the one which characterizes an isolated H_2 molecule of the same bond length. There is a driving force for contraction of the H_2 molecules in the interacting system. We can speak of *over-contracted H_2 molecules*. The H_2 molecules are trying to preserve their molecular character.

For lower values of r_s, from 1.1 to 0.9, the difference is becoming positive and more and more positive, indicating that while having the same bond length, the density at the bond critical point is lower in the interacting system than in the adapted isolated molecule. It indicates a driving force for partial dissociation. *Based on this argument, we can consider that H_2 molecules of the "3 H_2" system are polymerizing in this r_s regime, i.e. for 0.9 < r_s < 1.1*. The H_2 molecule character is lost, so in this phase we will speak of *dissociating H_2 entities*.

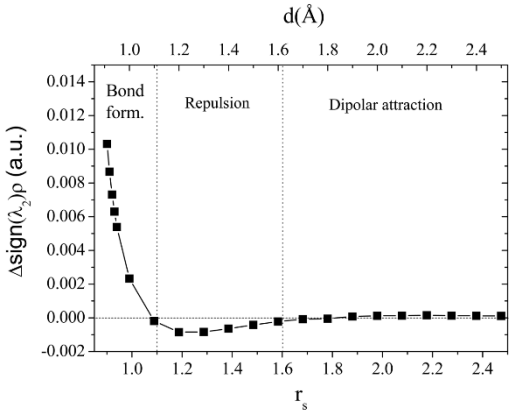

Figure 9. Difference between the sign(λ_2)ρ value of BCP #1 and that of an isolated H_2 molecule whose bond length has been adapted.

The evolution upon compression of the volume associated with the intermolecular interacting regions (regions #2 and #3 on Figure 6) is plotted in Figure 10. Upon compression, the volume of intermolecular interactions increases, first slowly from r_s = 2.5 to r_s = 2.0 (i.e. the r_s domain for which we have said that the corresponding pressures were lower than 1 atm) and

then more sharply from r_s = 2.0 to r_s = 1.6 (essentially the domain of perturbed true H_2 molecules). For r_s ranging from 1.6 to 1.0, (the domain of over-contracted H_2 molecules) the interacting volume almost reaches a plateau. Then, as r_s goes on decreasing and the H_2 entities are really dissociating the interacting volume decreases. This global evolution is consistent with a chemical reaction taking place. Indeed, in "classical" bimolecular chemical reactions consisting of a single elementary step, the transition state has been shown to be associated with a high interacting volume between the two chemical partners.[55] Based on this argument, and by analogy with a terminology used in chemical reactivity, rather than of over-contracted H_2 molecules, we can speak of *activated H_2 molecules*.

As one of the two intermolecular interactions is attractive (region #2) and the other one repulsive (region #3), the overall interacting volume can be divided into an attractive volume (blue lozenges curve on Figure 10) and a repulsive volume (red squares curve on Figure 10).

The attractive volume increases from r_s = 2.5 to r_s = 1.6, first slowly (for 2.0 < r_s < 2.5) then more sharply. It reaches its highest value at r_s = 1.6, i.e. at the r_s value for which the H_2 molecules begin to be activated. Then it decreases from r_s = 1.6 to r_s = 0.9. The repulsive volume increases regularly from r_s = 2.5 to r_s = 1.1-1.0. So it reaches its highest value when H_2 molecular entities begin to show signs of dissociation (elongation, electron density at the BCP smaller than for an adapted isolated molecule). Then it decreases from r_s = 1.0 to r_s = 0.9.

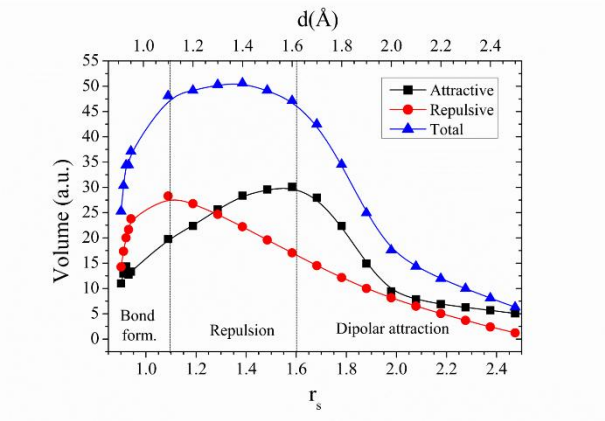

Figure 10. a) Volume (left) integrations within the NCI region (such as $-0.2 < \text{sign}(\lambda_2)\rho < 0.2$ a.u and $0.0 < s(\rho) < 2.0$ a.u), separated into attractive ($\lambda_2 < 0$) and repulsive ($\lambda_2 > 0$) contributions. The reference for the integrations is one H_2 molecule extracted from the "3 H_2" system for each r_s.

To summarize all these results, the progressive transformation of 3 quasi non-interacting H_2 molecules into an H_6 molecular entity made of 6 equivalent H-H bonds as the pressure increases can be divided into 4 steps (we ignore the $2.5 < r_s < 2.0$ domain which correspond to pressures lower than 1 atm):

- From $r_s = 2.0$ to $r_s = 1.6$, while dipolar attraction between the three H_2 molecules increases, the H_2 entities of the "3 H_2" system perturb each other. As a consequence, the H_2 molecules contract. Nonetheless the electronic distribution remains identical to that of a short isolated H_2 molecule; we can say that the H_2 molecules interact together mainly due to van der Waals interactions and are true H_2 molecules, only little perturbed with respect to isolated H_2 molecules. This regime is characterized by quasi prolate ELF isosurfaces. This is the *dipolar attraction regime*. Note that in this r_s regime -- it will be useful for the following -- the electron density at the BCPs corresponding to attractive intermolecular interactions increases from 0 to 0.006 a.u.

- From r_s = 1.6 to r_s = 1.1, driven by the dipolar attraction regime, the H_2 molecules respond by over-shortening and over-strengthening the H-H intramolecular bonds (electron density at the intramolecular BCP is higher than in an isolated H_2 molecule having the same bond length). As a consequence, the "attractive" interaction volume decreases. The ELF isosurfaces show a deformation towards the ring center with a retreat in the intermolecular regions. We can say that in this r_s regime the H_2 molecules attempt to preserve their H_2 molecular integrity by contracting. In the meantime, the "repulsive" interacting volume goes on increasing. This is the *repulsion regime*. Note that in this r_s regime the electron density at the BCPs corresponding to attractive interactions increases from 0.006 a.u. to 0.045 a.u.
- From r_s= 1.1 to r_s = 0.9, as the "repulsive" interacting volume has become too high, the H_2 molecules now elongate and the H-H intramolecular bonds are softened (electron density at the intramolecular BCP lower than in an isolated H_2 molecule having the same bond length). The ELF isosurfaces now show a retreat in the intramolecular region. H_2 molecules are partially dissociating (the electron density at the corresponding BCPs decreases from 0.255 a.u. to 0.170 a.u.) while in the same time new partial H-H bonds are formed in the "intermolecular" regions (the electron density at the corresponding BCPs increases from 0.045 a.u. to 0.170 a.u.). The initial H_2 molecules have lost their H_2 integrity. This is the r_s regime where the chemical reaction is effectively taking place with formation of new covalent bonds between the initial H_2 entities. This is the *bond formation regime.*
- Below r_s = 0.9 complete polymerization is reached and only one type of covalent bond is found (H_6 region). As r_s decreases the six equivalent H-H bonds shorten and strengthen. This is the *polymerized regime*.

2. Periodic models.

In order to evaluate the transferability of the conclusions drawn from the "3 H_2" system to 3D extended systems, an analogous NCI analysis (unfortunately without integrations of the electron density properties within the NCI regions, as this type of analysis is currently not available for periodic systems) was carried out on the 'best structures' for solid hydrogen proposed in [19] for P < 500 GPa. As a reminder, the *$P6_3/m$*, *C2/c*, *Cmca-12*, *Cmca* and *$I4_1/amd$* structures are presented in Table 1, with the pressure range for which they have originally be claimed to be that of lowest enthalpy (neglecting the zero point motion).

For each of these 5 structures, we studied the evolution of NCIs within their pressure range of stability. Figure 11 plots s(ρ) for each structure at pressures for which they were originally proposed to be the lowest enthalpy phase (P = 100GPa for *$P6_3/m$*, P = 250 GPa for *C2/c* , P = 350 GPa for *Cmca-12*, P = 490 GPa for *Cmca* and P = 500 GPa for *$I4_1/amd$*). Note that for the sake of clarity, the y-axis for $\lambda_2 < 0$ is shifted by +0.1 a.u.

As for the "3 H_2" system, we can identify three types of interactions in each periodic structure: covalent bonds, attractive and repulsive intermolecular interactions. Note that since the molecular periodic structures are characterized by several H_2 molecular entities, nonequivalent by symmetry, covalent bonds correspond to several s(ρ) peaks. Similarly, due to the presence of numerous nonequivalent neighbors for each H_2 molecule, the s(ρ) peaks corresponding to intermolecular interactions are numerous. Therefore, it appears more relevant, for a given structure at a given pressure, to associate a range of electron density values rather than a precise electron density value for each kind of interactions (data are reported in Table S5).

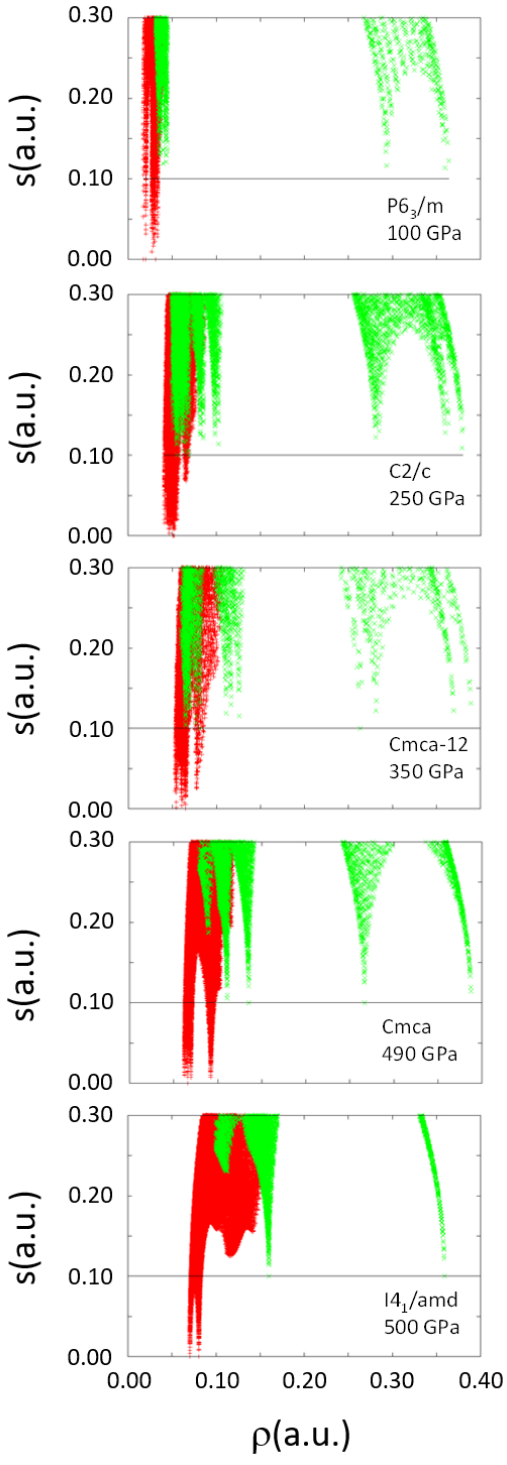

Figure 11. Plots of s(ρ) for hydrogen solids, $P6_3/m$, C2/c, Cmca-12, Cmca and $I4_1/amd$, at 100, 250, 350, 490 and 500 GPa, respectively ($\lambda_2 < 0$ in green and $\lambda_2 > 0$ in red). For the sake of clarity, the y-axis for $\lambda_2 < 0$ is shift of +0.1 a.u.

Figure 12 shows the evolution of electron density at BCPs as a function of pressure for each structure in their pressure range of stability. As in the "3 H_2" molecular system, the typical electron densities of both kinds of intermolecular (attractive and repulsive) interactions increase under compression, indicating a strengthening of the intermolecular interactions as the pressure increases. And as in the "3 H_2" molecular system, at a given pressure, attractive intermolecular interactions appear stronger than repulsive ones. Interestingly, upon compression, the electron density at BCPs associated with intermolecular interactions behaves in a very continuous manner, despite the 'transition' from one phase to another. Only small shifts are observed at the transition from the molecular *Cmca* structure to the monatomic $I4_1/amd$ one at P = 500 GPa.

As for the 'intramolecular' interactions, as the pressure increases, the electron density at BCPs first increases then decreases and finally increases again. This evolution is qualitatively the same as in the "3 H_2" system, though typical density values appear quite different. Indeed, at P ~250 GPa, the electron density at attractive intermolecular BCPs is typically 0.10 a.u and that at intramolecular BCPs about 0.281-0.285 a.u. For comparison, in the "3 H_2" system, at the r_s value for which the electron density at attractive intermolecular BCPs is also about 0.10 a.u., that at intramolecular BCPs is already as low as 0.23 a.u. Thus, it seems that in the 3D extended structures, the reinforcement of intermolecular interactions does not induce a weakening of the H-H intramolecular bonds as pronounced as in the "3 H_2" model system. The effect of the 3D confinement of the trimers probably stabilizes the deformed clouds better than our planar model. Nonetheless, the global picture of the evolution of interactions under compression drawn from the "3 H_2" molecular model is recovered in periodic structural models for solid hydrogen.

It is then very tempting to try to recover for periodic models the four steps of the polymerization process we deduced from the analysis of the "3 H_2" system. It would have

been very interesting to be able to do it from comparison of the r_s values. Unfortunately, it appears that there is no coincidence between the 1D r_s radius computed for the "3 H_2" system and the 3D r_s radius computed for the periodic structural models of dense hydrogen. Indeed, P = 1 atm corresponds to a 3D r_s values of 3.1 whereas we have already noticed that in the "3 H_2" system it was associated to $r_{s,1D}$ = 2.0. Therefore, we have to search for these four steps from other arguments.

Transition from the bond formation regime to the polymerized regime is maybe the easiest one to identify. Quite obviously, in our set of periodic models, it occurs at P = 500 GPa at the transition from the molecular *Cmca* phase to the monoatomic *$I4_1/amd$* one. Very interestingly, at P ~ 500 GPa, the typical electron density at BCPs of the *$I4_1/amd$* phase is 0.16 a.u. while in the "3 H_2" system, at the transition from the bond formation regime to the polymerized regime, it is almost the same: 0.17 a.u. As already mentioned, this final step is the only one leading to a jump in the electron density. Whereas the planar model is constrained to evolve in a continuous manner, bond changes in solid state are sudden in many cases. Still, electron density at 500 GPa for the *$I4_1/amd$* fits well with the model, which would mean that the last step of the "model" transformation is avoided. This points towards a reconstructive transition.

Transition from the dipolar attraction regime to the repulsion regime has been identified in the "3 H_2" system as the moment at which H_2 molecules over-strengthen with respect to shortened isolated H_2 molecules. This moment is reached before intramolecular H-H bond lengths reach their shortest value; so in our set of periodic models, it should occur below P = 100 GPa. If we focus on the typical electron density at the intermolecular BCPs (ρ = 0.006 a.u at $r_{s,1D}$ = 1.6 in the "3 H_2" system), it should occur at quite a low pressure, around P ~3 GPa.

Transition from the repulsion regime to the bond formation regime has been identified as the moment at which H_2 entities become weaker than an isolated elongated H_2 molecule. Based

on one hand on the evolution of the intramolecular distances in the periodic models (see Fig 7 in [25]) and on the other hand on Fig.12 it should happen around P = 250 GPa. At that pressure, the typical electron density at the intermolecular BCP is about 0.05-0.10 a.u.. In the "3 H_2" system, the electron density at the BCP is about 0.045 a.u at the transition from the repulsion regime to the bond formation regime ($r_{s,1D}$ ~1.1), close to the lower end of the range in the periodic system. So, it seems that the bond formation regime is delayed in 3D extended systems with respect to our "3 H_2" simple model, so that interactions can be stronger, and it is when the weakest one becomes "strong enough" that the transformation starts. Further studies are needed on this point, but it is a first hint on how to extend molecular laws/rules of chemical bonding to the periodic realm. It is in agreement with the fact that the 3D network stabilizes the repulsive regime and reinforces intermolecular interactions, so that pressure induces a smaller weakening of the H-H intramolecular bonds than the "3 H_2" model system. From another point of view, in periodic models, electron density at the attractive intermolecular BCPs first reaches a value of 0.045 a.u at around P ~100 GPa, which is also approximately the pressure at which experimentally the H_2 Raman vibron frequency becomes smaller than that characteristic of solid hydrogen at atmospheric pressure (see Fig. 7 in [56]). Therefore, the transition from the repulsion regime to the bond formation regime does not appear unambiguous, as if the formation of covalent bonds in place of the original intermolecular interactions was in advance with respect to the partial dissociation of the initial intramolecular bonds. The 3D network and numerous environments favors this shift, enhancing some intermolecular bonds more than other, as can be seen from one of the most apparent characteristics of Figure 12: as the polymerization is approached, the range of electron densities at the intermolecular BCPs greatly increases. All in all, hydrogen phase III definitely appears to belong to the bond formation regime. It can be seen as the phase where the chemical reaction of polymerization is effectively taking place.

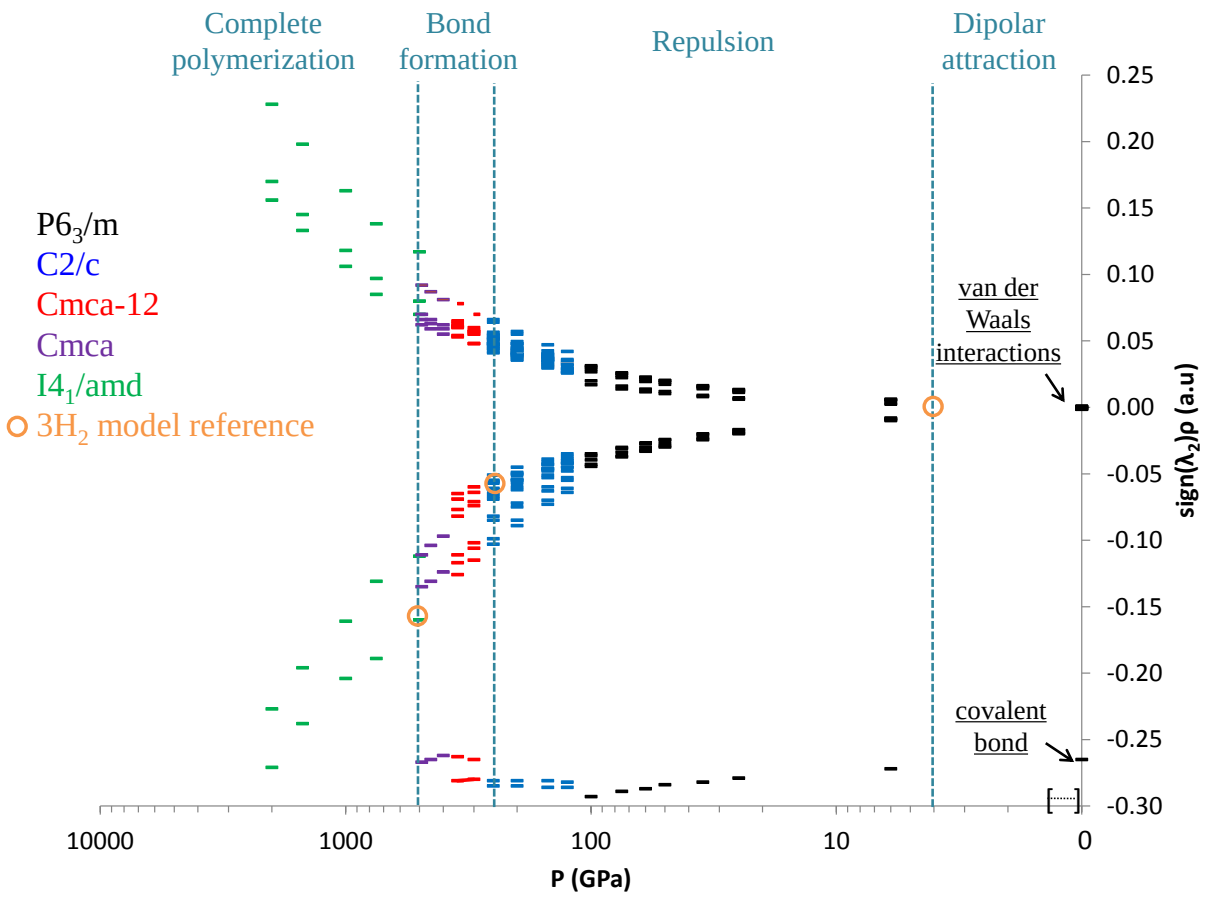

Figure 12. Evolution of main interactions within best candidates in function of the pressure (GPa).

6. Summary and conclusions.

To better understand the mechanism by which solid hydrogen polymerizes under pressure, we have first computationally analyzed the "$3H_2$" non-periodic molecular model in the imposed D_{3h} symmetry. The pressure effect was simulated by the variation of the r_s (d) value. Using a wide variety of wavefunction analysis, three transition regimes were highlighted prior to

polymerization: (*i*) The dipolar attraction region is characterized by van der Waals interactions between the H_2 covalently bound molecules. (*ii*) A repulsion region, where molecules deform and polarize, contracting, maintaining their nature (*iii*) bond formation, where molecules expand and lose their identity, becoming activated for the polymerization.

We have used the information derived from the model to understand the phase diagram of hydrogen and how it polymerizes. We have found that the model allows to reproduce the main changes observed in the molecular phases, with sequential contraction and expansion of H_2 molecules. Electron density at the critical points behaves rather continuously like in the cluster model along the first stages (electronic in nature) until final polymerization, where a strong reconstruction is expected.

We have used the stages in the model to identify the electronic nature of the molecular phases: $P6_3/m$ and C2/c belong to the repulsive phase whereas Cmca and Cmca-12 show characteristics of the bond formation stage. The latter phases show important characteristics of bond formation under solid which would help understanding bond formation and evolution under pressure: (i) the intermolecular bond formation is postponed with respect to the cluster model and (ii) numerous intermolecular contacts of different strength appear, which reflect the changing nature of the bond preparation. Both of these characteristics reflect the effect of the periodic 3D network not taken into account by the model.

Hence, with this combined cluster-periodic approach, we have been able to identify the electronic stages of polymerization, identify the reconstructive nature upon polymerization and characterize the effects of the 3D network.

SUPPORTING INFORMATION

MO diagram of $3H_2$ for point-group D_{3h}. Connection between the radius d and r_s. For all d values the NCI plots and isosurfaces of $3H_2$ system. NCI plots of isolated H_2. $3H_2$ molecular model cartesian coordinates calculated at the PBEPBE/6-311++G(d,p) level. Evolution of different energetic term under compression for $3H_2$: the SCF energy without and with dispersion energy, the total classical ionic-like interaction energy and the total exchange-correlation (covalent-like) interaction energy. Comparison of energies of ring of three H_2 molecules at the imposed D_{3h} and D_{6h} symmetry point-group as function of d. For the stability pressure range, NCI plots, completes isosurfaces, lattice parameters and atomic coordinates, energies, enthalpies, pV terms and volumes of hydrogen solid phases. Structural description and NCI evolution under pressure of solid phases. This material is available free of charge via the Internet at http://pubs.acs.org.

Present Addresses

†Institut Photovoltaïque d'Ile de France (IPVF), 8 rue de la Renaissance 92160 Antony, France and Institute for Research and Development of Photovoltaic Energy (IRDEP), UMR 7174 CNRS / EDF R&D / Chimie ParisTech-PSL, 6 quai Watier, 78401 Chatou, France

Notes

There are no conflicts of interest to declare.

ACKNOWLEDGMENTS

We thank Y. Ellinger for valuable discussions about CASSCF calculation.

REFERENCES

(1) McMillan, P.F. Chemistry at high pressure. *Chem. Soc. Rev.* **2006**, *35*, 855-857.

(2) Wigner, E.; Huntington, H.B. On the possibility of a metallic modification of hydrogen. *J. Chem. Phys.* **1935**, *3*, 764-770.

(3) Amaya, K.; Shimizu, K.; Eremets, M.I. Search for Superconductivity under Ultra-high pressure. *Int. J. Mod. Phys. B* **1999**, *13*, 3623-3625.

(4) Grochala, W.; Hoffmann, R.; Feng, J.; Ashcroft, N. W. The chemical imagination a work in very tight places *Angew. Chem. Int. Ed.* **2007**, *46*, 3620-3642.

(5) (a) Eremets, M.I.; Hemley, R. J.; Mao, H.-k.; Gregoryanz, E. Semiconducting non-molecular nitrogen up to 240 GPa and its low-pressure stability. *Nature* **2001**, *411*, 170-174; (b) Eremets, M. I.; Gavriliuk, A. G.; Trojan, I. A.; Dzivenko, D. A.; Boehler, R. Single-bonded cubic form of nitrogen. *Nature Mat.* **2004**, *3*, 558-563.

(6) (a) Iota, V.; Yoo, C. S.; Cynn, H. Quartzlike carbon dioxide: an optically nonlinear extended solid at high pressures and temperatures, *Science* **1999**, *283*,1510-1513. (b) Yoo, C. S.; Cynn, H.; Gygi, F.; Galli, G.; Iota, V.; Nicol, M.; Carlson, S.; Häusermann, D.; Mailhiot, C. Crystal structure of carbon dioxide at high pressure: "superhard" polymeric carbon dioxide. *Phys Rev. Lett.* **1999**, *83*, 5527-5530.

(7) Prewitt, C. T.; Downs, R. T. High-pressure crystal chemistry. *Rev. Mineral. Geochem.* **1998**, *37*, 283-317.

(8) Hemley, R. J. Percy W. Bridgman's second century *High. Press. Res.* **2010**, *30*, 581-619.

(9) Dias, R. P.; Silvera, I. F. Observation of the Wigner-Huntington transition to metallic hydrogen. *Science* **2017**, *355*, 715-718.

(10) (a) Goncharov, A. F.; Struzhkin, V. V. Comment on Observation of the Wigner-Huntington transition to metallic hydrogen. arXiv:1702.04246; (b) Eremets, M. I.; Drozdov, A. P. Comments on the claimed observation of the Wigner-Huntington transition to metallic hydrogen. arXiv:1702.05125; (c) Loubeyre, P.; Occelli, F.; Dumas, P. Comment on:

Observation of the Wigner-Huntington transition to metallic hydrogen. arXiv:1702.07192; (d) Silvera, I.; Dias R. Responses to critiques on observation of the Wigner-Huntington transition to metallic hydrogen. arXiv:1703.03064.

(11) Nellis, W. J. Wigner and Huntington: the long quest for metallic hydrogen. *High Press. Res.* **2013**, *33*, 369-376.

(12) Ashcroft, N. W. Metallic hydrogen: A high-temperature superconductor? *Phys. Rev. Lett.* **1968**, *21*, 1748-1749.

(13) Cudazzo, P.; Profeta, G.; Sanna, A.; Floris, A.; Continenza, A.; Massidda, S.; Gross, E. K. U. Ab initio description of high-temperature superconductivity in dense molecular hydrogen. *Phys. Rev. Lett.* **2008**, *100*, 257001(4).

(14) McMahon, J. M.; Ceperley, D. M. High-temperature superconductivity in atomic metallic hydrogen. *Phys. Rev. B* **2011**, *84*, 144515(8).

(15) Babaev, E.; Sudbo, A.; Ashcroft, N. W. A superconductor to superfluid phase transition in liquid metallic hydrogen. *Nature* **2004**, *431*, 666-668.

(16) Babaev, E.; Sudbo, A.; Ashcroft, N. W. Observability of a projected new state of matter: a metallic superfluid. *Phys. Rev. Lett.* **2005**, *95*, 105301(4).

(17) Howie, R. T.; Guillaume, C. L.; Scheler, T.; Goncharov, A. F.; Gregoryanz, E. Mixed molecular and atomic phase of dense hydrogen. Phys. Rev. Lett. 2012, 108, 125501.

(18) (a) Pickard, C. J.; Martinez-Canales, M. ; Needs, R. J. Density functional theory study of phase IV of solid hydrogen. *Phys. Rev. B* **2012**, *85*, 214114(8); (b) Pickard, C. J.; Martinez-Canales, M.; Needs, R. J. Erratum: Density functional theory of phase IV of solid hydrogen. *Phys. Rev. B* **2012**, *86*, 059902(1).

(19) Pickard, C. J.; Needs, R. J. Structure of phase III of solid hydrogen. *Nature Phys.* **2007**, *3*, 473-476.

(20) McMahon, J. M.; Ceperley, D. M. Ground state structures of atomic metallic hydrogen. *Phys. Rev. Lett.* **2011**, *106*, 165302(4).

(21) McMahon, J. M.; Morales, M. A.; Pierleoni, C.; Ceperley, D. M. The properties of hydrogen and helium under extreme conditions. *Rev. Mod. Phys.* **2012**, *84*, 1607-1653 and references within.

(22) Goncharov, A. F.; Howie, R. T.; Gregoryanz, E. Hydrogen at extreme pressures (Review article). *Low Temp. Phys.* **2013**, *39*, 402-408.

(23) Zha, C.-C.; Liu, Z.; Hemley, R. J. Synchroton infrared measurements of dense hydrogen to 360 GPa. Phys. Rev. Lett. 2012, 108, 146402(5).

(24) Loubeyre, P.; Occelli, F.; LeToullec, R. Optical studies of solid hydrogen to 320 GPa and evidence for black hydrogen. *Nature* **2002**, *416*, 613-617.

(25) Labet, V.; Gonzalez-Morelos, P.; Hoffmann, R.; Ashcroft, N. W. A fresh look at dense hydrogen under pressure. I. An introduction to the problem, and an index probing equalization of H-H distances. *J. Chem. Phys.* **2012**, *136*, 074501(14).

(26) Labet, V.; Hoffmann, R.; Ashcroft, N. W. A fresh look at dense hydrogen under pressure. II. Chemical and physical models aiding our understanding of evolving H-H separations. *J. Chem. Phys.* **2012**, *136*, 074502(10).

(27) Labet, V.; Hoffmann, R.; Ashcroft, N. W. A fresh look at dense hydrogen under pressure. III. Two competing effects and the resulting intra-molecular H-H separation in solid hydrogen under pressure. *J. Chem. Phys.* **2012**, *136*, 074503(10).

(28) Liu, H.; Zhu, L.; Cui, W.; Ma, Y. Room-temperature structures of solid hydrogen at high pressures. *J. Chem. Phys.* **2012**, *137*, 074501(7).

(29) Liu, H.; Wang, H.; Ma, Y. Quasi-molecular and atomic phases of dense solid hydrogen. *J. Phys. Chem. C* **2012**, *116*, 9221-9226.

(30) Drummond, N. D.; Montserrat, B.; Lloyd-Williams, J. H.; Lopez Rios, P.; Pickard, C. J.; Needs, R. J. Quantum Monte Carlo study of the phase diagram of solid molecular hydrogen at extreme pressures. *Nature Comm.* **2015**, *6*, 7794(6).

(31) Pickard, C. J.; Needs, R. J. Ab initio random structure searching. *J. Phys.: Condens. Matter* **2011**, *23*, 053201(23).

(32) Momma, K.; Izumi, F. VESTA 3 for three-dimensional visualization of crystal, volumetric and morphology data. *J. Appl. Cryst.* **2011**, *44*, 1272-1276.

(33) In our previous study (Ref[26], the ring radius *d* was chosen as the distance between the center of the ring and the middle of each H_2 molecular entity. In the present study, *d* has been chosen to be the distance between the center of the ring and each proton, as shown in Figure 1.

(34) Wiberg, K. B. Application of the Pople-Santry-Segal CNDO method to the cyclopropylcarbinyl and cyclobutyl cation and to bicyclobutane. *Tetrahedron*, **1968**, *24*, 1083-1096.

(35) (a) Bader, R. F. W. A quantum theory of molecular structure and its applications. *Chem. Rev.* **1991**, *91*, 893-928; (b) Bader R. F. W. The quantum mechanical basis of conceptual chemistry. *Monatsh. Chem.* **2005**, *136*, 819-854; (c) Bader R. F. W. Atoms in molecules: A

quantum theory (The international series of monographs on chemistry, 22). Oxford University Press Inc., New York, 1994.

(36) Becke, A. D.; Edgecombe, K. E. A simple measure of electron localization in atomic and molecular systems. *J. Chem. Phys.* **1990**, *92*, 5397-5403.

(37) (a) Silvi, B.; Savin, A. Classification of chemical bonds based on topological analysis of electron localization functions. *Nature* **1994**, *371*, 683-686; (b) Savin, A.; Nesper, R.; Wengert, S.; Fässler T. F. ELF: The Electron Localization Function. *Angew. Chem. Int. Ed. Engl.* **1997**, *36*, 1808-1832.

(38) Johnson, E. R.; Keinan, S.; Mori-Sanchez, P.; Contreras-Garcia, J.; Cohen, A. J. ; Yang, W. Revealing noncovalent interactions. *J. Am. Chem. Soc.* **2010**, *132*, 6498-6506.

(39) Boto, R. A.; Contreras-Garcia, J.; Tierny, J.; Piquemal, J.-P. Interpretation of the reduced density gradient. *Mol. Phys.* **2016**, *114*, 1406-1414.

(40) Contreras-Garcia, J.; Johnson, E. R.; Keinan, S.; Chaudret, R.; Piquemal, J.-P. ; Beratan, D. N.; Yang, W. NCIPLOT: A program for plotting noncovalent interaction regions. *J. Chem. Theory Comput.* **2011**, *7*, 625-632.

(41) Contreras-Garcia, J.; Yang, W.; Johnson, E. R. Analysis of hydrogen-bond interaction potentials from the electron density : integration of noncovalent interaction regions. *J. Phys. Chem. A*, **2011**, *115*, 12983-12990.

(42) Gaussian 09, Revision **D.01**, M. J. Frisch, G. W. Trucks, H. B. Schlegel, G. E. Scuseria, M. A. Robb, J. R. Cheeseman, G. Scalmani, V. Barone, B. Mennucci, G. A. Petersson, H. Nakatsuji, M. Caricato, X. Li, H. P. Hratchian, A. F. Izmaylov, J. Bloino, G. Zheng, J. L. Sonnenberg, M. Hada, M. Ehara, K. Toyota, R. Fukuda, J. Hasegawa, M. Ishida, T. Nakajima,

Y. Honda, O. Kitao, H. Nakai, T. Vreven, J. A. Montgomery, Jr., J. E. Peralta, F. Ogliaro, M. Bearpark, J. J. Heyd, E. Brothers, K. N. Kudin, V. N. Staroverov, R. Kobayashi, J. Normand, K. Raghavachari, A. Rendell, J. C. Burant, S. S. Iyengar, J. Tomasi, M. Cossi, N. Rega, J. M. Millam, M. Klene, J. E. Knox, J. B. Cross, V. Bakken, C. Adamo, J. Jaramillo, R. Gomperts, R. E. Stratmann, O. Yazyev, A. J. Austin, R. Cammi, C. Pomelli, J. W. Ochterski, R. L. Martin, K. Morokuma, V. G. Zakrzewski, G. A. Voth, P. Salvador, J. J. Dannenberg, S. Dapprich, A. D. Daniels, Ö. Farkas, J. B. Foresman, J. V. Ortiz, J. Cioslowski, and D. J. Fox, Gaussian, Inc., Wallingford CT, 2009.

(43) Grimme, S. Semiempirical GGA-Type Density Functional Constructed with a Long-Range Dispersion Correction. *J. Comput. Chem.* **2006**, *27*, 1787-1799.

(44) Grimme, S.; Antony, J.; Ehrlich, S.; Krieg, S. A consistent and accurate ab initio parametrization of density functional dispersion correction (DFT-D) for the 94 elements H-Pu. *J. Chem. Phys.* 2010, 132, 154104(19).

(45) MOLPRO, version 2012.1, a package of *ab initio* programs, H.-J. Werner, P. J. Knowles, G. Knizia, F. R. Manby, M. Schütz, P. Celani, T. Korona, R. Lindh, A. Mitrushenkov, G. Rauhut, K. R. Shamasundar, T. B. Adler, R. D. Amos, A. Bernhardsson, A. Berning, D. L. Cooper, M. J. O. Deegan, A. J. Dobbyn, F. Eckert, E. Goll, C. Hampel, A. Hesselmann, G. Hetzer, T. Hrenar, G. Jansen, C. Köppl, Y. Liu, A. W. Lloyd, R. A. Mata, A. J. May, S. J. McNicholas, W. Meyer, M. E. Mura, A. Nicklass, D. P. O'Neill, P. Palmieri, D. Peng, K. Pflüger, R. Pitzer, M. Reiher, T. Shiozaki, H. Stoll, A. J. Stone, R. Tarroni, T. Thorsteinsson, and M. Wang, see http://www.molpro.net.

(46) Roos, B. O.; Taylor, P. R.; Siegbahn, P. E. M. A complete active space SCF method (CASSCF) using a density matrix formulated super CI approach. *Chem. Phys.* **1980**, *48*, 157-173.

(47) Noury, S.; Krokidis, X.; Fuster, F.; Silvi, B. Computational tools for the electron localization function topological analysis. *Computers & Chemistry* **1999**, *23*, 597-604.

(48) Blöchl, P. E. Projected augmented-wave method. *Phys. Rev. B* **1994**, *50*, 17953-17979.

(49) Kresse, G.; Joubert, D. From ultrasoft pseudopotentials to the projector augmented-wave method. *Phys. Rev. B* **1999**, *59*, 1758-1775.

(50) Kresse, G.; Hafner, J. Ab initio molecular dynamics for liquid metals. *Phys. Rev. B* **1993**, *47*, 558-561.

(51) Kresse, G.; Furthmüller, J. Efficiency of ab-initio total energy calculations for metals and semiconductors using plane-wave basis set. *Comput. Mater. Sci.* **1996**, *6*, 15-50.

(52) Kresse, G.; Furthmüller, J. Efficient iterative schemes for ab initio total-energy calculations using a plane-wave basis set. *Phys. Rev. B* **1996**, *54*, 11169-11186.

(53) (a) Perdrew, J. P.; Burke, K.; Ernzerhof, M. Generalized Gradient Approximation made simple. *Phys. Rev. Lett.* **1996**, *77*, 3865-3868; (b) Perdrew, J. P.; Burke, K.; Ernzerhof, M. ERRATA Generalized Gradient Approximation made simple. Phys. Rev. Lett. 1997, 78, 1396-1396.

(54) Otero-de-la-Roza, A. ; Contreras-Garcia, J. ; Johnson, E. R. Revealing non-covalent interactions in solids : NCI plots revisited. *Phys. Chem. Chem. Phys.* **2012**, *14*, 12165-12172.

(55) Andres, J.; Berski, S.; Contreras-Garcia, J.; Gonzalez-Navarrete, P. Following the molecular mechanism for the NH3 + LiH → LiNH2 + H2 chemical reaction: a study based on the joint use of the quantum theory of atoms in molecules (QTAIM) and noncovalent interaction (NCI) index. *J. Phys. Chem. A* **2014**, *118*, 1663-1672.

(56) Mao, H.-k.; Hemley, R. J. Ultrahigh-pressure transitions in solid hydrogen. *Rev. Mod. Phys.* **1994**, *66*, 671-692.